# The galactic chemical evolution of carbon: Constraining stellar nucleosynthesis

Daniel A. Boyea,[1] et al.
[1]*Department of Astronomy, The Ohio State University*
[2]*Department, Institution, Street Address, City Postal Code, Country*
[3]*Another Department, Different Institution, Street Address, City Postal Code, Country*

Accepted XXX. Received YYY; in original form ZZZ

**ABSTRACT**

Stellar evolution models provide highly uncertain predictions for elemental yields due to our limited understanding of stellar physics. In this paper, we aim to estimate the nucleosynthetic yields of carbon using galactic chemical evolution models.

We find that the AGB stars make up a fraction $0.20^{+80}_{-20}$ of total carbon production at late times.

**Key words:** Need to find some...

## 1 INTRODUCTION

Where does each chemical element come from?

Stellar evolution models can be used to predict how much of each element stars with a variety of physical properties produce. However, these models are rife with uncertainties, limited by our understanding of critical physical processes such as nuclear reaction rates, convection, opacity, and mass loss (CITE, e.g. stellar physics reviews).

Carbon and nitrogen are well studied elements as they are easy to observe (Citations...). Additionally, carbon and nitrogen are used as age indicators for giant branch stars (citations, e.g. Vincenzo et al. (2021)), and are the only light elements known to be produced significantly in Asymptotic Giant Branch Stars (AGB) (cite).

However, theoretical interpretations of the trends of

While easily visible in many stars, determining birth abundances of carbon and nitrogen are

One challenge of measuring abundances of carbon in star is that when a star becomes a RGB star, material from the CNO-processed core. Since this core-processed material is now carbon depleted and nitrogen enhanced, measurments of this star's atmosphere will no longer reflect the birth abundances of the star. Additionaly, carbon is extremelt challenging to measure gas-phase abundances for because the strongest visible line is ...., e.g. carbon unreliable in GALAH, low detections.

AGB stars are known to be importaint (cite) from stellar model predictions, previous GCE, and evidence from abundance patterns. (are there detections in PN?)

Core Collapse Supernovae (CCSNe) are also important (.... SN reminant measurments)

We also know that there is evidence for non-monatonic carbon yield patterns. pattern where carbon is more readily produced by both high metallicity and very low metallicity stars (CEMPS, early GCE results), but our picture.

Additionally, stellar models are computationally expensive, even in one dimension, so while there are grids of predictions, these are not always fine enough to make accurate chemical evolution models.

In Fig. 1 we present a sample of APOGEE subgiants. These subgiants were chosen based on their location in the HR diagram based on criteria in Roberts et al. (2023) replicated in Appendix A. Because subgiants have not undergone FDU, their surface abundances are an accurate reflection of the birth abundances (CITATION).

## 2 NUCLEOSYNTHESIS

Modern theoretical nucleosynthesis provides our starting point for our models. We focus on three primary nucleosynthetic pathways: AGB stars, CCSne, and SNeIa. Each process has unique timescales and element production which we can trace through the tools of GCE. While carbon is only known to be produced in AGB stars and CCSNe, comparing carbon to iron production (from SNeIa) adds a valuable constraint to our models and insight into the delay-time production of carbon.

After a group of stars are formed, CCSNe from massive stars are the first enrichment, providing light elements such as C, O, and Mg and heavier elements such as Fe and beyond. Importaintly, $\alpha$ elements like O and Mg are only formed in CCSNe (in significant quantities). Next, low mass stars begin to reach the end of their lives. The dying breaths of AGB stars are known to be importaint sources of C, N, and a smattering of heavier elements. Finally, the white dwarfs, including formation and time to collide/over-eat, explode, releasing much of Fe and nearby elements.

We focus on O and Mg as $\alpha$ elements only formed in CCSNe, and use Fe to trace delayed enrichment from SNeIa. C and N are both formed in AGB and CCSNe.

There are two $\alpha$-elements we care about: Mg and O. Stellar observations of magnesium are more reliable but oxygen abundances are easier to measure in HII regions. We assume that both Mg and O are produced entirely in CCSNe with constant, metallicity-independent yields. Thus [Mg/H] = [O/H] = [$\alpha$/H] in our models. (Observational validation?)

For carbon, the dominant producer is from massive stars which eject carbon fused in their cores during CCSNe.

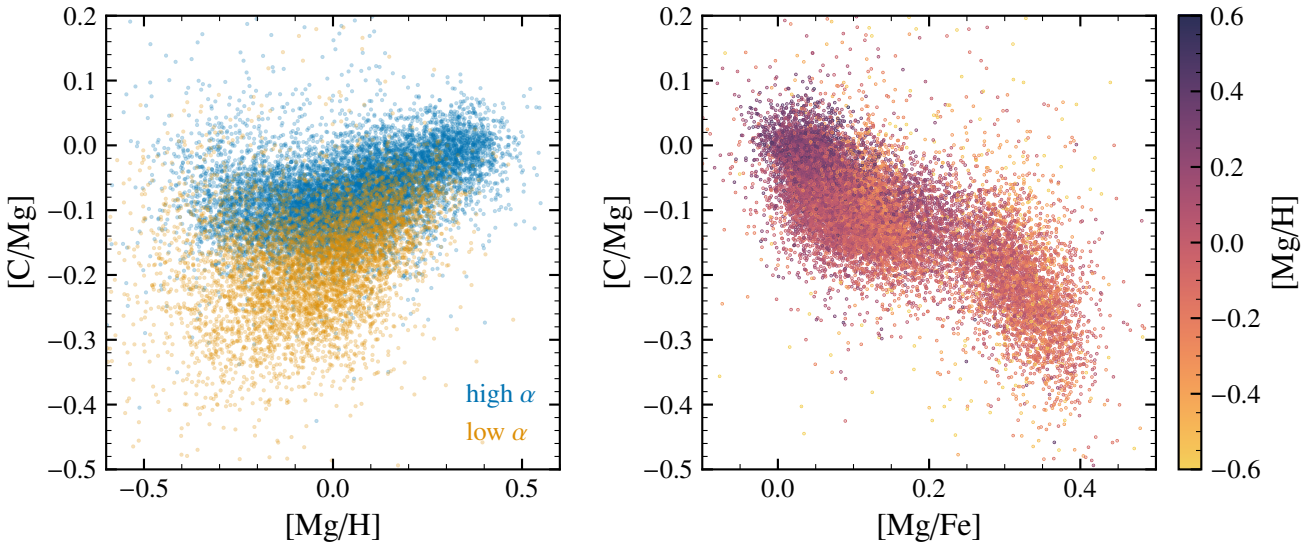


**Figure 1.** The [C/Mg] ratio against [Mg/H] (left) and [Mg/Fe] (right). The left panel uses blue and orange to represent high and low $\alpha$ sequences respectively. On the right, we plot more metal rich ([Mh/H]) stars with darker colors.

As we focus on the yields of carbon, we keep yields for other elements fixed in most models. Taken from Johnson et al. (2021, 2022), we let

- $Y_{\rm O}^{\rm CC} = 0.015$
- $Y_{\rm O}^{\rm Ia} = 0$
- $Y_{\rm Fe}^{\rm Ia} = 0.00214$?
- $Y_{\rm Fe}^{\rm CC} = 0.0012$
- $Y_{\rm N}^{\rm CC} = 0.00036$
- $y_{\rm N}^{\rm AGB}(M, Z) = 9 \times 10^{-4} M \left(\frac{Z}{Z_\odot}\right)$

Also following Johnson et al. (2021, 2022), we take the SNeIa Delay Time distribution to be a $t^{-1.1}$ law suggested by the observations of Maoz et al. (2012).

### 2.1 Asymptotic giant branch carbon

An AGB star is a low mass ($\lesssim 8 M_\odot$) star during the final phases of evolution. In an AGB star, two competing processes determine the outcome of carbon production. Third Dredge Up (TDU) is needed to eject carbon from the star, enriching the surface with helium-burning-processed material from the core. But Hot Bottom Burning (HBB) at the base of the convection layer changes carbon into nitrogen. TDU occurs during thermal pulsations, where the convective layer of the star passes into the inner layers with He-burning products which mixes in C and O into the envelope. In contrast, HBB may happen if the base of the convective envelope reaches about 50MK, initiating the CNO cycle, converting most C12 into N14.

Carbon abundances are strongly affected by CNO cycle processing in stars. The CNO cycle is one of two series of nuclear reactions( $^{12}$C(p, $\gamma$)$^{13}$N($\beta^+\nu_e$)$^{14}$N(p, $\gamma$)$^{15}$O($\beta^+\nu_e$)$^{15}$N(p,$\alpha$)$^{12}$C

Because the $^{14}$N(p, $\alpha$) proton capture is the slowest component of the CNO cycle ****, the CNO cycle, to first order, converts all $^{12}$C into $^{14}N$.

The differences in yields between AGB models depend on the mass loss rate, treatment of convection, and nuclear reaction rates.

In this work, we explore four different sets of AGB star yields representative of the variety of options which also provide reasonably well sampled grids in metallicity and mass necessary for chemical evolution studies.

- Cristallo et al. (2011) and Cristallo et al. (2015) (C11+C15).
- Karakas (2010) (K10)
- Ventura et al. (2013) V13
- Karakas & Lugaro (2016) Karakas et al. (2018) KL16+K18

Unless otherwise noted, C11 is the model we choose as our fiducial AGB yield.

We use IMF-Integrated yields calculated with `VICE` throughout this paper (see section 3, Johnson et al. (2021, 2022)). For an element X and star with mass $M$, the stellar yield $y$ is defined as the net production of X relative to $M$, or

$$y_{\rm X} = \frac{M_{\rm X,\ ejected} - Z_{0,X} M_{\rm ejected}}{M} \tag{1}$$

where we let $M_{\rm ejected}$ and $M_{\rm X,ejected}$ be the total ejected stellar mass (through winds and supernovae ejecta) and the ejected mass of X, and $Z_{0,X}$ was the birth mass fraction of element X.

More useful for GCE are Initial Mass Function (IMF) yields, where we sum up the contributions of all stars which produce an element. We define the IMF-integrated yield of X with:

$$Y_{\rm X}^{\rm proc}(Z) = \int_{M_{\rm min}}^{M_{\rm max}} y_{\rm X}^{\rm proc}(M, Z)\ \Phi(M)\ dM \tag{2}$$

Where $\Phi(M) = \frac{dN}{dM} / \int_{M_{\rm min}}^{M_{\rm max}} \frac{dN}{dM}\ dM$ is the normalized IMF, $M_{\rm min}$ and $M_{\rm max}$ are the minimum and maximum mass of stars, which we take to be $0.08 M_\odot$ and $100 M_\odot$ respectively; and $\frac{dN}{dM}$ is the initial mass function, the frequency of stars born between $M$ and $M + dM$.

Fig. 2 compares the net fractional AGB carbon yield, $m_{\rm C}^{\rm AGB}(M, Z)$ for each AGB model we consider. Note that the yields may be negative when the birth abundance is higher than the carbon abundance of the material ejected back to the ISM.

Most models agree on the qualitative shape of the net fractional AGB carbon yield. The stars with the highest fractional carbon yields are between 2 to 4 solar masses, depending on the metallicity and model. Both lower and higher mass stars produce less carbon, and

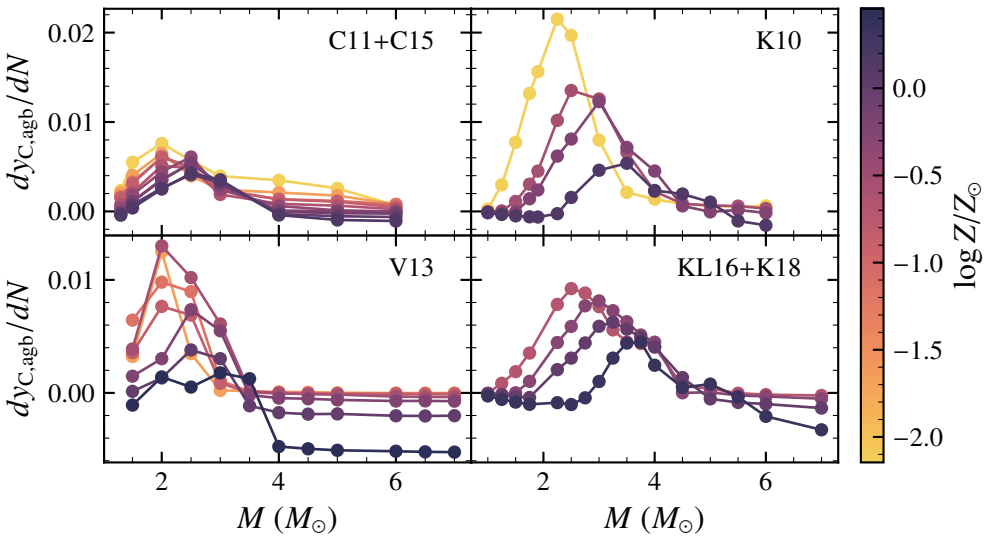


**Figure 2.** The net fraction carbon yield ($M_C$, the amount of carbon produced by the star divided by $M$) plotted as a function of mass, $M$. Lighter colors represent higher values of metalicity ([M/H]). Each panel represents a different AGB model. K10 reports stars at MoverH -3, -2, etc. I can reproduce C11 and K10 but not other V13 and KL16 :(((

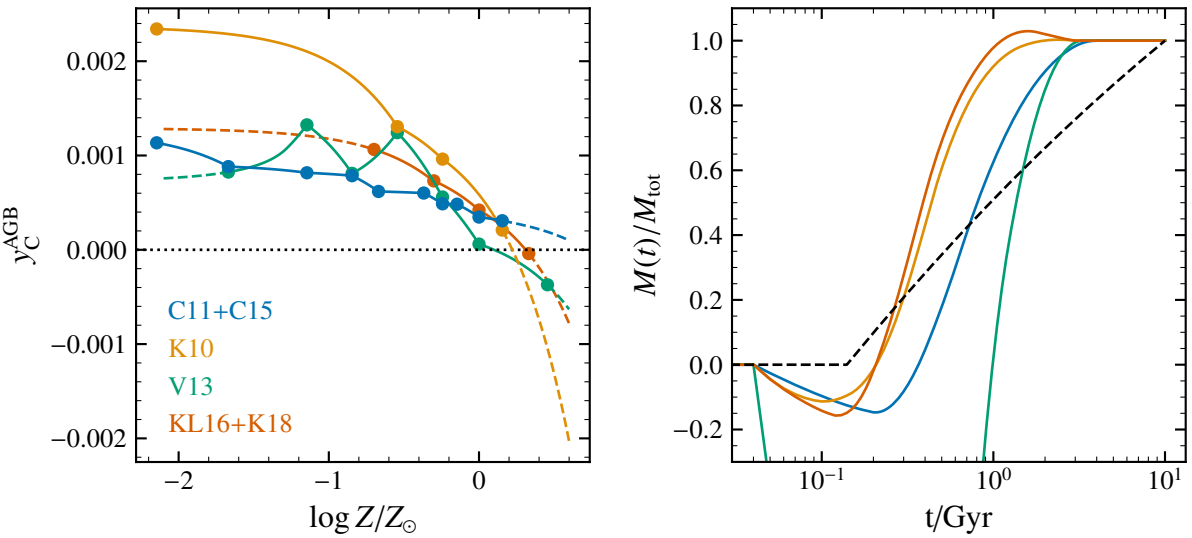


**Figure 3.** On the left, we plot the IMF weighted net fractional carbon yields of each AGB model as a function of metalicity.The right panel plots the normalized net carbon AGB yield as a function of time for a population of stars born at the same time at solar metallicity. We note that for the right panel, the minimum of the DTD for V13 is

high mass stars may even destroy carbon at high metallicity due to highly efficient HBB. And all models agree that the carbon yield generally decreases with metallicity.

Metallicity dependence: V13 is the only model that stands out, showing a non-monotonic metallicity dependence, however this effect is only for models with [M/H]$\leq -1$. Otherwise the major differences between the models are the precise amount of carbon and the slope of the metallicity dependence. For example, the three models C11, K10, and K16 predict $y_C^{AGB}$ to be between 0.006 and 0.008 at solar metallicity, but C11 has a much shallower metallicity dependence than the K10 and K16 models. And at solar, V13 predicts a value at around 0.004 so the models are all within about a factor of 2.

Another difference is the speed at which equilibrium is reached. K10 and K16 weight carbon production more heavily towards massive stars resulting in a faster time to equilibrium, whereas the C11 and V13 models predict a slightly longer timescale with order 1Gyr, but little to no carbon is produced more than 2Gyr after a star formation event. This is in contrast to iron which is still produced by SNeIa up to 10Gyr after a star formation event.

### 2.2 CCSNe carbon

While there are many stellar models providing predictions of CCSNe yields, the results of these models are highly uncertain due to the many stellar modeling uncertainties.

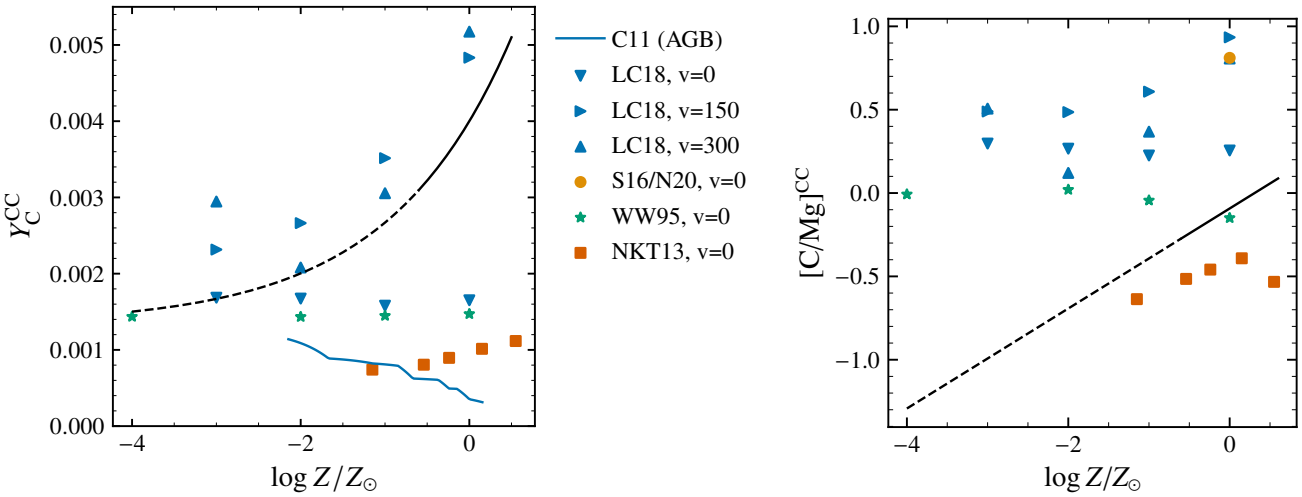


**Figure 4.** The fist plot shows IMF-weighted net fractional CCSNe yield of carbon, $y_C^{cc}$ against metalicity, [M/H], for different studies. The right plot instead shows $[C/O]^{CC}$, the logarithm of the abundance ratio of carbon to oxygen if CCSNe were the only carbon source, also as a function of metallicity for the same set of studies. The black line represents the carbon yield of the fiducial model, $y_C^{CC} = 0.004?(Z/Z_\odot)^{0.3}$, and becomes dashed over regions where we have not tested our model.(Nomoto et al. 2013), (Limongi & Chieffi 2018), (Sukhbold et al. 2016), (Woosley & Weaver 1995)

We summarise many of the predictions of stellar models in Fig. 4.

$$[C/O]^{CC} = \log_{10}\left(\frac{y_C^{CC}}{y_O^{CC}}\right) - \log_{10}\left(\frac{Z_{C,\odot}}{Z_{O,\odot}}\right) \tag{3}$$

Notice how even these ratios

- Wide range in predictions, exacerbated to 1 dex range when including variance in oxygen predictions
- (explain) most models have a near-metallicity independent oxygen yield, so we choose the fiducial value of 0.015 despite varience in $y_O^{cc}$
- The fiducial value, where we choose the carbon yield from Sukhbold+16, may be above most predictions of carbon yields but is within the range of yield ratios
- the fiducial value would reach an equilibrium carbon yield of -0.1 without AGB stars
- Rotation in LC18 appears to increase metallicity dependence of carbon production (read this paper more carefully)
- NKT and LC agree in positive metallicity depenent yields

## 3 THE MULTIZONE MODEL

To simulate the chemical evolution of a Milky-Way-like galaxy, we use the Versitile Integrator for Chemical Evolution (`VICE`[1]) published in Johnson et al. (2021) and also briefly described in Johnson et al. (2022). As a multi-zone model, the galaxy is divided into 200 rings of 0.1kpc, each with separate gas supplies with outflow and inflow rates.

`VICE` accounts for radial migration by using the results of the `h277` hydrodynamical simulation. Each VICE SSP is matched to a random nearby star particle *analogue* in `H277`. VICE approximates the migration of this particle by using a $\sqrt{\text{time}}$-diffusion approximation where the change in galactic radius of a star, $\Delta R$, is $\Delta R \propto \sqrt{t}$. VICE does not account for radial gas flows.

[1] `VICE` is available at `https://github.com/giganano/VICE`

Other approaches have used dynamical arguments to implement their stellar mirgrations. We note that our approach does not introduce more free parameters which may bias conclusions. However, we only consider one dynamic history, and it is still unknown how variations in the dynamic history of a galaxy impact its chemical evolution.

We initially assume an "inside-out" SFH where the star formation rate peaks in the early evolution of the galaxy and is higher closer to the galactic center. The star formation rate, $\Sigma_\star$, for our fiducial model is parameterized by

$$\dot{\Sigma}_\star \propto \left(1 - e^{-t/\tau_{\text{rise}}}\right) e^{-t/\tau_{\text{sfh}}} \tag{4}$$

where $\tau_{\text{rise}} = 2$Gyr is the and $\tau_{sfh}$ is the rate of decline of the star formation rate, which is based on *****.

We also explore a "lateburst" model which is parameterized with a normal distribution multiplying our fiducial "inside-out" SFH as

$$\dot{\Sigma}_{\text{lateburst}} \propto \dot{\Sigma}_{\text{insideout}} \left(1 + Ae^{-(t-\tau_{\text{burst}})^2/2\sigma^2_{\text{burst}}}\right) \tag{5}$$

$A = 1.5$ represents the amplitude of the birth, $\tau_{\text{burst}} = 10.8$Gyr is the time where the burst is strongest, and $\sigma_{\text{burst}} = 1$Gyr is the width of the burst. We do explore the effects of variations of this parameterization in section ****.

VICE normalizes the total mass of star formation against observations from ******. The gas inflow is calculated based on our star formation parameterization by using a schmit law

$$dM_g \propto \dot{\Sigma}^{1/n} \tag{6}$$

where we take $n$ to be ****

Salpeter IMF.

### 3.1 Model Stellar Yields

We define a parameterization of a CCSNe yield Because of the large uncertainties in CCSNe carbon yields, we choose to explore an analytic expression of the yield enabling us to easily explore how variations of CCSNe carbon yields affect abundance tracks. We find that a powerlaw yield with a metallicity-dependent constant

minimum is able to match the observations well while remaining a simple parameterization (see below). Our expression is:

$$Y_{\rm C}^{\rm CC}(Z) = \alpha\ Z^{\beta} Y_{\rm O}^{\rm CC} + Y_{\rm C,\,0}^{\rm CC} \tag{7}$$

Where we estimate $\alpha = 0.02$ and $\beta = 0.25$ (See Section 5 ). Our second model uses $\alpha = 0.44$ and $\beta = 0.63$ with K16 yields and reduced $\eta \rightarrow 1/2\eta$

As an overall scaling of yields does not significantly affect our models, we choose to fix the total equilibrium value of the total carbon yield at solar at $Y_{\rm C,\,\odot} = 0.005$, and then scale the yields relative to this value.

## 4 MULTIZONE MODEL RESULTS

### 4.1 Data Selection

We use data from APOGEE DR17 (Majewski et al. 2017) processed with APOSCAP. Since subgiant stars have yet to experience FDU, their atmospheric carbon and nitrogen abundances are still reflective of their birth abundances and do not need mixing corrections.

To select for subgiants, we use the following cut in $\log g$ and $T_{\rm eff}$ which selects stars at the base of the red giant turnoff (FIGURE and Roberts et al. (2023)). We describe our selection criteria along with a comparison to Vincenzo et al. (2021) in Appendix A.

Because the star formation history is left in a simple inside-out form, this multizone model does not reproduce the high-$\alpha$ sequence, therefore we make the following cut to the V21 data to remove the high alpha sequence.

$$\begin{cases} [\rm Mg/Fe] > 0.12 - 0.13[\rm Fe/H], & [\rm Fe/H] < 0 \\ [\rm Mg/Fe] > 0.12, & [\rm Fe/H] > 0 \end{cases} \tag{8}$$

While we show the entire dataset in Fig. 1, we chose to compare the binned data to our models as black points with dashes representing the 1-sigma spread, as in e.g. Fig. 6.

### 4.2 The Evolution of carbon across the galaxy and through time

The GCE of carbon is complicated by metallicity dependencies and delayed contributions.

We note the following features of our model:

(i) Carbon comes predominantly ($\sim$ 80%) from CCSNe but the rest is from AGB stars

(ii) The CCSNe carbon production is more efficient at higher metallicities

(iii) AGB stars produce less carbon at higher metallicities.

The combination of these features leads to an evolution that proceeds as follows

(i) Initially, CCSNe dominate production before AGB stars can contribute their enrichment, but because CCSNe is highly metallitiy dependent, the C/$\alpha$ ratio increases with time.

(ii) AGB stars begin contributing their carbon, increasing the $C/\alpha$ ratio more steeply as the gas begins to reach its equilibrium metallicity

(iii) When $Z$ reaches equilibrium, the $C/\alpha$ ratio stops increasing or may even decline, as AGB stars formed at higher metallicities reduce the net carbon yields.

**Table 1.** For each AGB yield set, our calculation of the effective SFH- and IMF-weighted carbon AGB yield, along with the multiplicative factor to reach an AGB contribution of 20.

| Study | $y_{\rm C,0}^{\rm agb}$ | $\alpha_{\rm agb,20}$ |
|---|---|---|
| C11 | 0.000347 | 2.9 |
| K10 | 0.000585 | 1.7 |
| V13 | 0.000060 | 16.5 |
| K16 | 0.000421 | 2.4 |

We plot time evolution tracks in Fig. 4.2 for [C/Mg]-[Mg/H]and [C/Mg]-[Mg/Fe]for our fiducial model. Each colored track corresponds to a different galactic radius and 1Gyr time steps are marked with crosses on the lines.

Comparing [C/$\alpha$] against [Fe/H] enables us to see late time evolution of carbon more clearly. Because [Fe/H] takes longer to reach equilibrium as half of iron production comes from type-Ia supernovae, the late time evolution is not clustered as tightly horizontally as for [$\alpha$/H].

This is even more evident in the lower part of Fig. 4.2, where we instead plot snapshots of the galactic radial trend at different times for our model. While the [C/Mg]-[Mg/H]trend reaches almost equilibrium at 5Gyr, the [C/Mg]-[Mg/Fe]trend continues to evolve even until the present day, exposing the effect of the delayed contribution from AGB stars on the evolutionary history.

### 4.3 Effects of AGB Yields

What happens as we change our choice of AGB stellar yields? We consider four models using the published yields in C11+C15, K10, KL16+K18, and V13 in Fig. 6.

As we chose to leave $Y_{\rm C}^{\rm CC}$ in a functional form, we chose to leave the total IMF-averaged carbon yield to be constant. The magnitude of $Y_{\rm C}^{\rm CC}$

$$Y_{\rm C}^{0} = 0.005 = Y_{\rm C}^{\rm cc} + Y_{\rm C}^{\rm agb}\Big|_{Z=Z_{\odot}} \tag{9}$$

where we are choosing to evaluate the total IMF CCSNe and AGB yields at solar metallicity. We show our calculations of $Y_{\rm C}^{\rm agb}(Z = Z_{\odot})$ in Table 1.

This choice of total carbon yield with our fixed choice of oxygen gives an equilibrium value of $Z_{\rm C}/Z_{\rm O} = Y_{\rm C}/Y_{\rm O} = 0.333$ which is reasonably consistant with the value in Asplund et al. (2009) of $Z_{\rm C}/Z_{\rm O} = 0.413$ and was chosen as to match the median value of our sample at $Z = Z_{\odot}$.

As the highest AGB yield at solar is from our K10 model at $Y_{\rm C}^{\rm agb} = 0.000585$ is only 11.7 percent of our required total carbon production, each of these models is dominated by CCSNe production of carbon. As a result, while the metallicity dependence of the [C/Mg]-[Mg/H]may vary, the [C/Mg]-[Mg/Fe]diagnostic shows how this small AGB fraction makes the details of the AGB model and delay-time-distribution unchange the galaxy production of carbon.

Appendix B describes the effects of increasing the AGB model on resulting abundance trends. However, we use the C11+C15AGB yields for the rest of the main discussion.

Our next exploration is to adjust the relative fraction of AGB star yields. To do this, we hold the total carbon yield at solar metallicity fixed, so for a desired AGB fraction (assuming equilibrium),

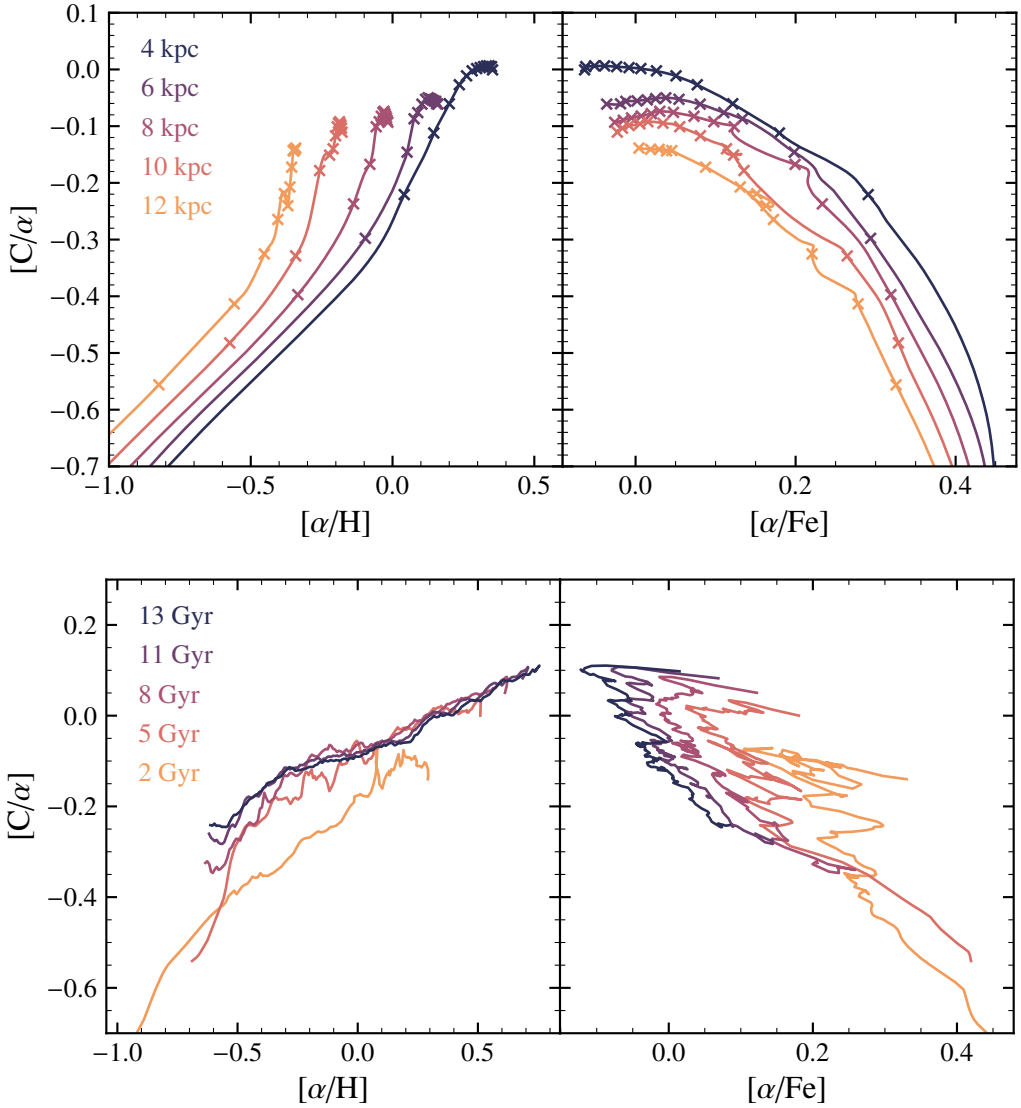


**Figure 5.** The top set of panes show the time evolution of the gas phase of our fiducial model, plotted as tracks through [C/Mg]-[Mg/H]and [C/Mg]-[Mg/Fe]where each colored line corresponds to the evolution at that galactic radius. The bottom set instead shows the galaxies gas-phase [C/Mg]-[Mg/H]and [C/Mg]-[Mg/Fe]trend at 5 different time slices.

$$\alpha_{\rm agb} = f_{\rm agb} \frac{y^{\rm tot}_{\rm C,0}}{y^{\rm agb}_{\rm C}} \tag{10}$$

$$\alpha_{\rm CC} = (1 - f_{\rm agb}) \frac{y^{\rm tot}_{\rm C,0}}{y^{\rm cc}_{\rm C}} \tag{11}$$

### 4.4 Metallicity dependence and the AGB Fraction

The next question is how does changing the CCSNe carbon yield affect the model? We now consider variations of our fiducial model:

- $f_{\rm agb} = 0.2$
- AGB model: C11+C15
- $Z^{\rm cc}_{\rm C} = 0.004(Z/Z_\odot)^{0.4}$ ($\beta = 4$)

We could chose to vary the value of $\alpha$; however, the overall scaling of yields is unknown so our constraint is really that $Y_{\rm C}/Y_{\rm O} = 0.dfsjkhld$, based on binning from our data. As discussed in the previous section, we chose to leave the total value of the IMF integrated yield fixed, and then assert the AGB fraction (next section) and scale the AGB yields from literature appropriety. As such,

As we display in Fig. 4.4, we observe that changes in $\beta$ are appropriety reflected in the resulting [C/Mg]-[Mg/H] trend. As the metallicity dependence steepens with higher $\beta$, the [C/Mg] ratio becomes correspondingly more dependent on [Mg/H].

Wow! Equilibrium!! See section 5

Importantly, the [C/Mg]-[Mg/Fe]trend is mostly unaffected by choosing a different CCSNe yield. As all CCSNe enrichment happens at the same, rapid timescale, by taking a slice in [Mg/H], this metallicity dependence is effectively ignored as the only effect can be a vertical offset if the slice is narrow enough.

So, the scaling of the trend and metallicity dependence of carbon

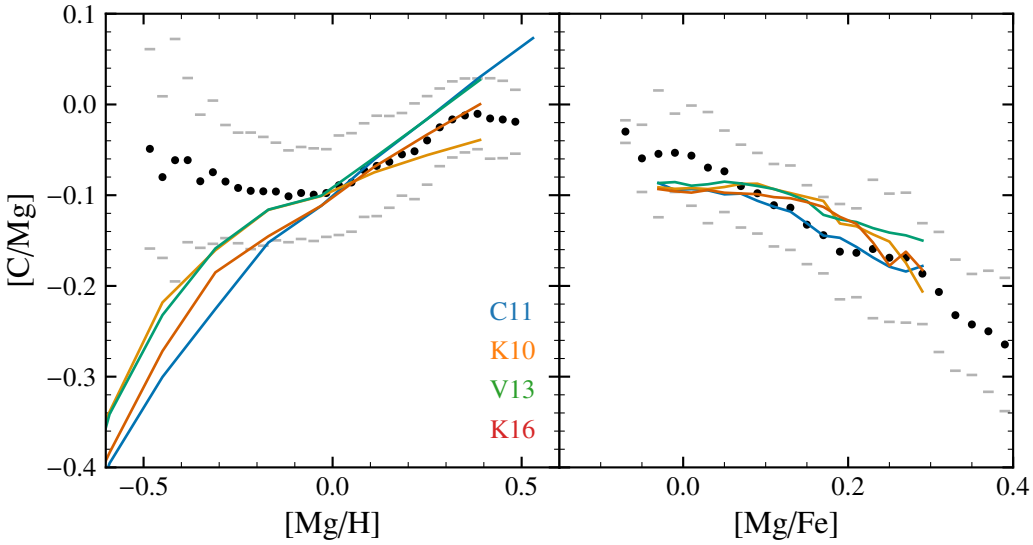


**Figure 6.** Left: the [C/Mg]-[Mg/H] **median** present-day stellar tracks for four different AGB models (C11+C15, K10, KL16+K18, and V13). The median bin [C/Mg] values from Roberts et al. (2023) are plotted as black points with 1-std errors marked by horizontal grey dashes. Right: same as left but for [C/Mg]-[Mg/Fe]. While each AGB yield model may differ in detail, there is minimal effect on the overall [C/Mg] trends.

(as seen in the [C/Mg]-[Mg/H] trend) gives information on the total carbon yield and the behavior of CCSNe (as the dominating producer of carbon); the [C/Mg]-[Mg/Fe]trend exposes the delayed effect of carbon from AGB contribution.

One caveat is that the slope of this trend is also determined by the ratio of delayed iron to CCSNe iron production as well. If the SNeIa iron fraction is increased, then more iron enters later reducing the slope of the trend as AGB becomes a more rapid mechanism than Fe comparatively. The difference however is that changing the Fe franction mostly affects the tail of the distribution as this controls the speed of descent off the high $\alpha$ sequence, but the AGB fraction even changes the behavior for the low $\alpha$ sequence.

### 4.5 The AGB Fraction

One potential tension with data is our models predict a low value for the AGB fraction of stars.

Our model with Z-dependent CCSNe yields has $f_{\rm agb} = 0.05$ which implies that CCSNe overwhelms AGB production and there should not be a seperation between low and high alpha sequences. However, V21 observes a significant seperation implying a more substantial delayed-time source.

Even changing the AGB model does not affect the conclusion significantly.

An alternate solution is to reduce the outflows and core collapse yields similarly, consistent with a model where more large stars collapse directly into black holes. This leaves the $y_{\rm C}^{\rm CC}/y_{\rm O}^{\rm CC}$ ratio unchanged, but because $y_{\rm C}^{\rm CC}$ is unchanged, the relative size of the AGB contribution is larger.

Increasing the relative AGB production lowers the magnitude of $y_{\rm C}^{\rm CC}/y_{\rm O}^{\rm CC}$, but the metallicity dependence of the ratio must increase to compensate for the inverse metallicity dependence of AGB carbon yields.

These models are indistinguishable in the [C/Mg]-[Mg/H] plane from our adjusted CCSNe model, so future work investigating the SFH and carbon isotopic ratios in more depth may be able to provide more insight. In the next section, we develop the analytic tools to explore this problem in more depth.

### 4.6 Star Formation History

We consider a simple modification of our SFH described by our lateburst model (see Equation 5)

equation of lateburst

However, we find that the star formation history has a negligable effect on the shape of the mean track. More drastic changes in SFH could explain the high alpha/low alpha seperation but we leave further exploration of SFH to future work.

### 4.7 Outflows

A common degeneracy in chemical evolution models is the yield-outflow degeneracy. An increase in stellar yields has a near-identical effect as a decrease in outflows. However, reducing the outflows reduces the evolution timescale of the system.

The theoretical motivation for decreasing outflows is due to the uncertainty in the explodability landscape—if less massive stars explode, then both the yields and outflows will be reduced by some factor. So, when we explore reduced outflow models, we consider models where both the outflows and yields are reduced by approximately the same factor, to leave the equilibrium abundances of a pure CCSNe unchanged.

The effect of reducing outflows is then increasing the relative contributions of non-CCSNe processes. For carbon, this increases the AGB fraction.

We have found that the [C/Mg]-[Mg/H] relationship may provide insight into this issue. [O/Fe] is a tracer of the relative contributions of CCSNe and delayed-time sources in chemical evolution. So, the appearance of a slope in [O/Fe] implies that there is a substantial delay-time process in carbon evolution. The metallicity-dependence of carbon yields complicates this picture because younger stars have higher [O/Fe] as the SNeIa contributions take up to 10Gyr, so metal-poor young stars will naturally have lower [C/O], agreeing with the

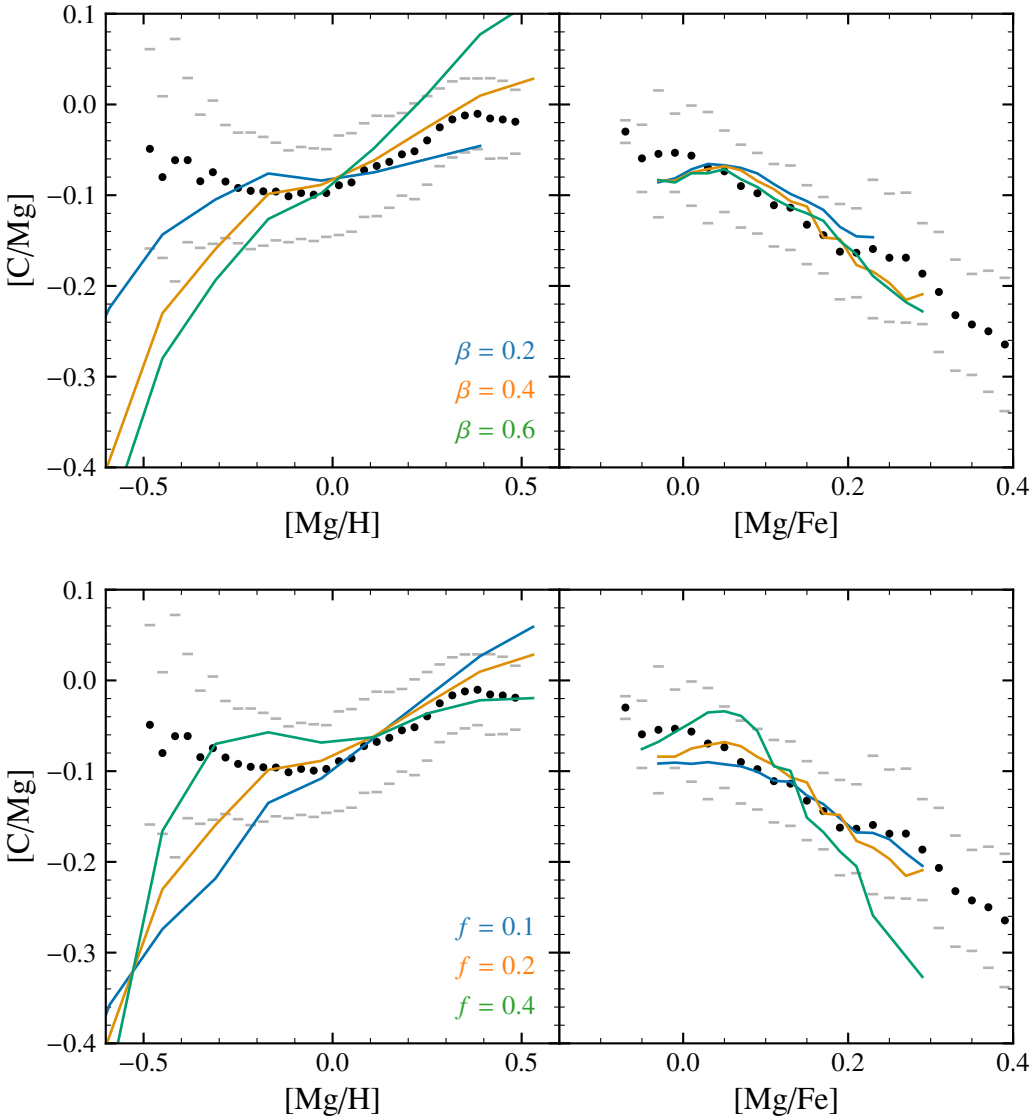


**Figure 7.** Similar to 6 except the top plot shows the fiducial model with lower and higher values of $\beta$, the C-CCSNe metallicity dependence. The bottom plot is the same except shows varying AGB fractions.

slope observed in[C/Mg]-[Mg/Fe]. However, a pure CCSNe carbon model cannot reproduce the slope accurately as

We find that we can adjust both the outflows and scale down the yields if we change our model for $y_{\rm C}^{\rm CC}/y_{\rm O}^{\rm CC}$. For example, reducing outflows and CCSNe yields by a factor of two requires the modified parameters $\alpha = 0.033$ and $\beta = 0.625$, which results in a slightly lower value at solar but nearly a doubling of the metallicity dependence.

### 4.8 Understanding Scatter

Beyond simply comparing median trends, we can compare the distribution shape of our distribution to observations.

### 4.9 Comparison to Observations

Beyond Milky Way stars, astronomers have observed carbon to oxygen ratios in HII-regions through either Recombination Lines or (OTHER TEchnique0), enabling us to probe gas-phase abundances of carbon in our galaxy and other types of galaxies from dwarf to elliptical.

In Fig. 10, we plot our fiducial model's gas phase abundances at present day and 2Gyr compared to C/O abundances measured in both stars, our subgiant sample, halo stars, galaxies, and even Damped Lynman Alpha (DLA) systems.

Our model appears to be broadly consistant with the gas phase data, however these imply if anything that the slope should be increased.

Are HII regions a good approximation?

Measuring carbon in the gas phase is challenging. Carbon emission lines are very weak compared to other common lines, (visible/etc.). Temperature/modelining limitations. Lack of strong HII calibration.

Short discussion of measurment challenges in extragalactic galaxies, how other galaxies and dwarf SFH may come into play, why this relation is notecably steeper.

Our model fails to capture the trend past [$\alpha$/H]= $-1$. As our knowledge of stellar evolution is limited, our knowledge of extremely metal poor stellar evolution is extremely limited. (despite a pure

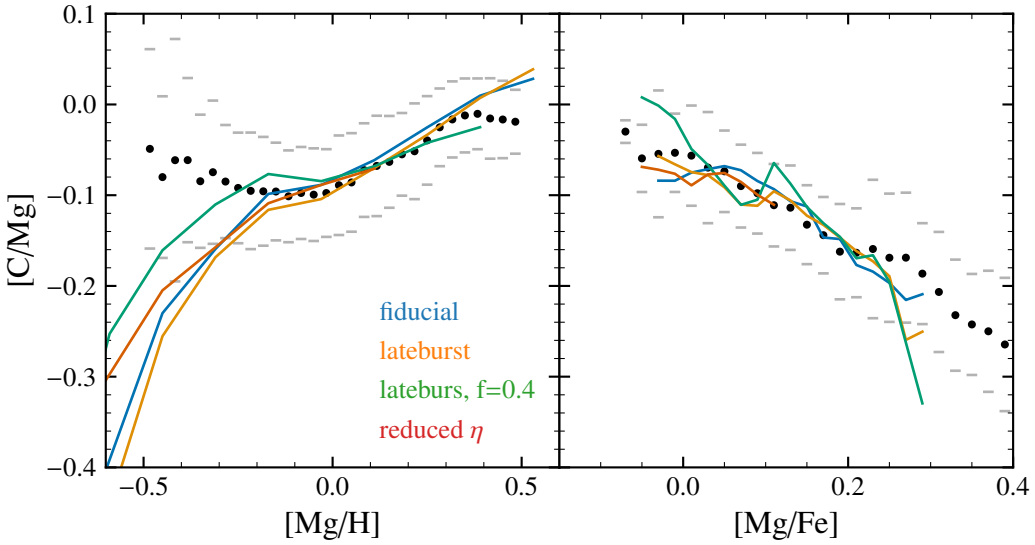


**Figure 8.** Same as Fig. 6 but comparing the fiducial model to the reduced outlow model and a lateburst model. (okay, need to totally change approach...)

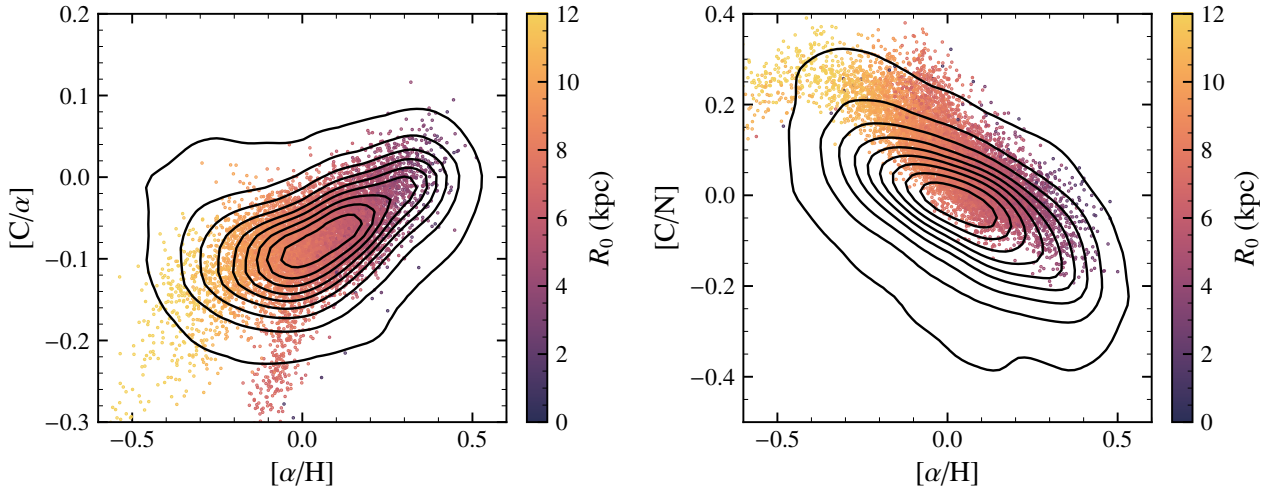


**Figure 9.** The simulated stars of our model at present day plotted on [C/Mg]-[Mg/H] and colored such that lighter colors represent stars born at greater galactric radii.

H/He born star appearing simpler lolol). A variety of explanation for the increasing relative carbon enrichments for metal-poor stars have been proposed (e.g. ...). The likely case that Population III star supernovae produced high abundances of carbon seems most plausable, especially given our uncertainty in the carbon yields and the short timescales required to create this enhancement (e.g. $z \sim 2$ DLA, dwarfs, etc.) make it unlikely that AGB stars could be the culprit.

As any constraints in this regieme are poor, we choose to only qualitatively conclude that CCSNe carbon production increases at extremely low metallicity but the details of this remains an open question.

Can we use our yield estimations and apply them to extragalactic sources successfully?

Explain Berg+19,

Bursty SFH may not be needed to explain scatter as the C/O slope + differet evolutionary timescales is capable alone of reproducing this scatter.

While the extragalactic trend appears to be more steeply sloped than our models, this is because of ***e.g. mass-dependent outflow rates/differening SFH between galaxies.

## 5 THE EQUILIBRIUM APPROXIMATION

If we assume that the median track is an equilibrium phenomenon, we can calculate the total carbon to oxygen yield ratio. Additionally, assuming an AGB yield set enables us to predict the CCSNe carbon yield. We begin with the model, which underlies the multizone simulations, that the change in mass of an element is a sum of production, outflows, recycling, and mass left in reminants. We write this as

$$M_{\rm C} = y_{\rm C}\dot{M}_\star - (1 + \eta - r)Z_{\rm C}\dot{M}_\star \tag{12}$$

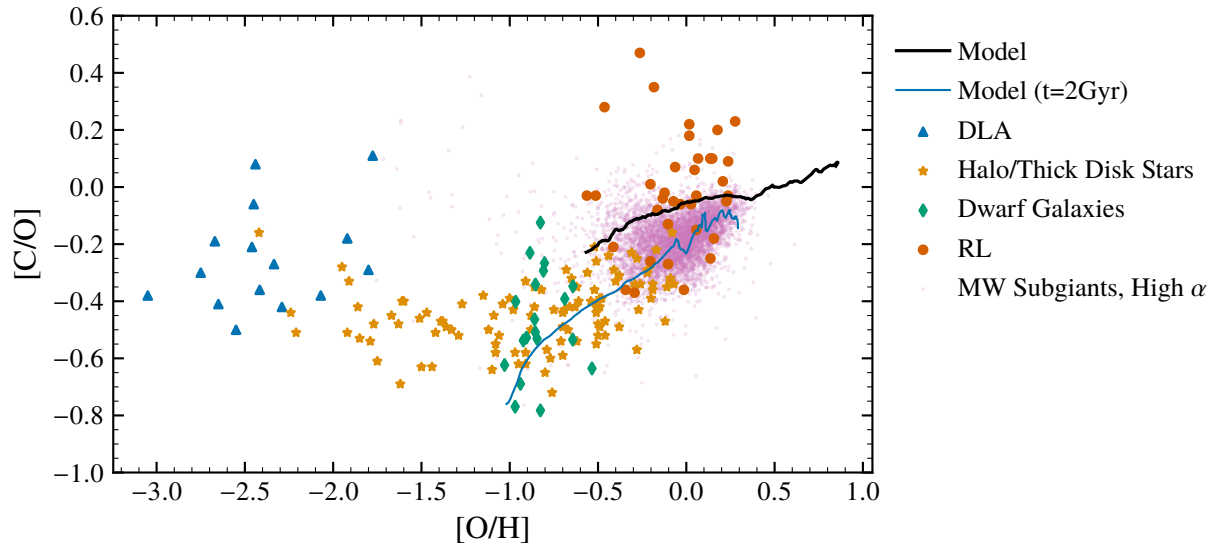


**Figure 10.** Present-day gas phase tracks of the fiducial model in [C/Mg]-[Mg/H] space. M101 is valid comparison to MW ...(van Dokkum et al. 2014)

In the case that carbon

$$Z_c^{eq}(R) = \frac{y_c^{cc} + \langle y_c^{agb} \rangle}{1 + \eta(R) - r - \tau_\star/\tau_{sfh}} \tag{13}$$

Where

$$\langle y_c^{agb} \rangle = \frac{\int_0^T y_c^{agb}(M,Z)\dot{M}_\star(T-t)\frac{dN}{dM}\frac{dM}{dt}dt}{\dot{M}_\star \int_0^T \frac{dN}{dM}\frac{dM}{dt}dt} \tag{14}$$

Likewise for oxygen:

$$Z_O^{eq}(R) = \frac{y_O^{cc}}{1 + \eta(R) - r - \tau_\star/\tau_{sfh}} \tag{15}$$

However, for the yield ratio, the denominator cancles with that of oxygen, so the ratio is fixed.

$$\frac{Z_c^{eq}}{Z_o^{eq}} = \frac{y_c^{cc} + \langle y_c^{agb} \rangle}{y_o^{cc}} \tag{16}$$

For this analysis, we let $y_c^{agb}$ represent the default AGB yields from a given yield set, but add a process factor $\alpha_{agb}$ which multaplicatively increases the AGB fraction. See Table 1.

$$y_{\rm C}^{\rm CC} \rightarrow \alpha_{agb} y_{\rm C}^{\rm CC} \tag{17}$$

With these definitions, we can calculate the core collapse yields of carbon as a function of metallicity:

$$y_{\rm C}^{\rm CC} = y_{\rm O}^{\rm CC}\frac{Z_{\rm C,eq}}{Z_{\rm O,eq}} - \alpha_{agb}\langle y_c^{agb} \rangle \tag{18}$$

Rewriting in terms of the observed abundance ratio and dividing by $y_{\rm O}^{\rm CC}$. So, given the outflows or CCSNe oxygen yields, the carbon AGB yield, and the [C/Mg]-[Mg/H]mean abundance track, we can estimate the CCSNe carbon yield. Written as a relative yield:

$$\frac{y_{\rm C}^{\rm CC}}{y_{\rm O}^{\rm CC}} = \frac{Z_{C,\odot}}{Z_{O,\odot}} 10^{[C/O]} - \frac{\alpha_{agb}\langle y_c^{agb} \rangle}{y_{\rm O}^{\rm CC}} \tag{19}$$

This equation corroberates what we have explored earlier in the paper, and provides our analytic estimates of the CCSNe carbon yields.

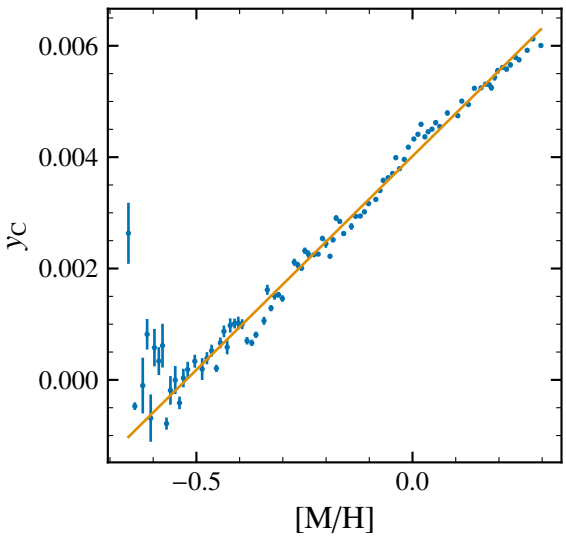


**Figure 11.** Our reverse fitting method to determine total CCSNe contribution

Since the AGB term is subtracted, a negative AGB Z-dependence will correspond to a positive CC Z-dependence. And as we reduce outflows, the AGB factor increases, steepening the required slope of the carbon yields. So, while the AGB yields may agree with eachother, the uncertainties in the oxygen CC yields and outflows leads to a substantial uncertainty in the AGB fraction.

$$y_C = (0.004 \pm 0.00002) + (0.008 \pm 0.0001)[\text{M/H}] \tag{20}$$

### 5.1 Uncertainties

We only perform this analysis on the C11/15 yields because the range of metallicities of the data (about [M/H] = -0.4, 0.4) only represents about 2 AGB models, relying heavily on our choice of extrapolation. C11/C15 have a finer model grid, allowing us to have 5 theoretical

predicted points within this metallicity range, allowing us to be more certain of our conclusion.

We do note that this analysis fails to take into account selection effects and biases in APOGEE, and a more robust determination of the carbon yield.

This formulation is degenerate in $\varpi$ until we estimate a better AGB fraction. As the seperation between the low and high alpha sequences can be used to estimate the delayed time contribution to carbon, using the model to estimate this value relies heavaly on the details of the SFH in addition to the We do give an estimate of the CCSNe yields, however this is dependent on our choice of $\eta$. Other choices of $\eta$ vary the value significantly in both magnitude and slope (as AGB contributions increase, we need less CCSNe carbon, however the CCSNe carbon must have a higher metallicity dependence to replicate the V21 data).

## 6 CONCLUSIONS

Directions–>SneIa/AGB trends as a constraint on DTD. Observations of Carbon in metal poor stars, extragalactic (call out any existing surveys in e.g. APOGEE/DESI?) Abundance ratios (e.g.C12/C13) as additional constraints

## ACKNOWLEDGEMENTS

The Acknowledgements section is not numbered. Here you can thank helpful colleagues, acknowledge funding agencies, telescopes and facilities used etc. Try to keep it short.

Numpy, pandas, scipy, VICE, matplotlib Harris et al. (2020); Hunter (2007)

Ohio Supercomputer Center (1987)

## DATA AVAILABILITY

The inclusion of a Data Availability Statement is a requirement for articles published in MNRAS. Data Availability Statements provide a standardised format for readers to understand the availability of data underlying the research results described in the article. The statement may refer to original data generated in the course of the study or to third-party data analysed in the article. The statement should describe and provide means of access, where possible, by linking to the data or providing the required accession numbers for the relevant databases or DOIs.

## REFERENCES

Asplund M., Grevesse N., Sauval A. J., Scott P., 2009, ARA&A, 47, 481
Cristallo S., et al., 2011, ApJS, 197, 17
Cristallo S., Straniero O., Piersanti L., Gobrecht D., 2015, ApJS, 219, 40
Harris C. R., et al., 2020, Nature, 585, 357
Hunter J. D., 2007, Computing in Science & Engineering, 9, 90
Johnson J. W., et al., 2021, MNRAS, 508, 4484
Johnson J. W., Weinberg D. H., Vincenzo F., Bird J. C., Griffith E. J., 2022, arXiv e-prints, p. arXiv:2202.04666
Karakas A. I., 2010, MNRAS, 403, 1413
Karakas A. I., Lugaro M., 2016, ApJ, 825, 26
Karakas A. I., Lugaro M., Carlos M., Cseh B., Kamath D., García-Hernández D. A., 2018, MNRAS, 477, 421
Limongi M., Chieffi A., 2018, ApJS, 237, 13
Majewski S. R., et al., 2017, AJ, 154, 94
Maoz D., Mannucci F., Brandt T. D., 2012, MNRAS, 426, 3282
Nomoto K., Kobayashi C., Tominaga N., 2013, ARA&A, 51, 457
Ohio Supercomputer Center 1987, Ohio Supercomputer Center, http://osc.edu/ark:/19495/f5s1ph73
Roberts J. D., Johnson J. A., Pinsonneault M. A., Others 2023, Nature vs nurture: Quantifying the carbon and nitrogen abundances of subgiant and red giant stars, in prep.
Sukhbold T., Ertl T., Woosley S. E., Brown J. M., Janka H. T., 2016, ApJ, 821, 38
Ventura P., Di Criscienzo M., Carini R., D'Antona F., 2013, MNRAS, 431, 3642
Vincenzo F., et al., 2021, arXiv e-prints, p. arXiv:2106.03912
Woosley S. E., Weaver T. A., 1995, ApJS, 101, 181

## APPENDIX A: VALIDATING THE APOGEE SUBGIANT SAMPLE

Our APOGEE subgiant sample excludes stars marked with the following flags:

- `ancillary young embedded cluster`
- `ancillary emission line star`
- `MIR-deected candidate cluster member`
- `selected as part of the EB program`
- `selected as part of the young cluster study (in-SYNC)`
- `W3/4/5 star forming complex`

To select stars only in the subgiant branch, we select stars in a polygon in $\log g$-$T_{\rm eff}$ space described by the following cuts:

$$\begin{cases} \log g \geq 3.5 \\ \log g \leq 0.004\, T_{\rm eff} - 15.7 \\ \log g \leq 0.00070588\, T_{\rm eff} + 0.358836 \\ \log g \leq -0.0015\, T_{\rm eff} + 12.05 \\ \log g \geq 0.0012\, T_{\rm eff} - 2.8 \end{cases} \tag{A1}$$

Instead of excluding stars which have experienced FDU and thus modified carbon abundances as JACK's subgiant sample does, another approach to predict the birth abundances of carbon and nitrogen in stars is to model the predicted abundance effects of dredge up and then correct the measured abundances, as is done in V21.

## APPENDIX B: EFFECTS OF ALTERNATE AGB MODELS

While we focus the main discussion of the paper on the C11 model, other AGB models can have notable effects on abundance trends at ***

Because the predictions of the AGB yield models we consider are dwarfed by the required CCSNe carbon production to match observations (see Fig. ***), we briefly explore here the effects of variations in AGB models affect abundance trend predictions when these models are amplified to match observational [C/MG]-[Mg/Fe] trends.

While most models are well represented by our AGB-fraction formalism, V13 presents a challenge as the predicted solar yield is much lower than the lower metallicity predictions, requiring the solar value to be a certain fraction forces us to amplify the yields by an unreasonable about (of order 10-30times) to reach the same $f_{\rm AGB}$ as other models. Thus, we instead calculate $f_{\rm AGB}$ at a metallicity of ... for this model.

V13 is also interesting as at high metallicity, the yields quickly become strongly negative. This causes a reversal of the [C/Mg]-[Mg/Fe] trend at high [Mg/H] slices (figure ...). As our set of observations do not appear to reverse, this indicates that carbon yields likely stay positive even at slightly super-solar, so models like V13 are a poor match to observations. Plot of age metallicity relationship?

This paper has been typeset from a TEX/LATEX file prepared by the author.

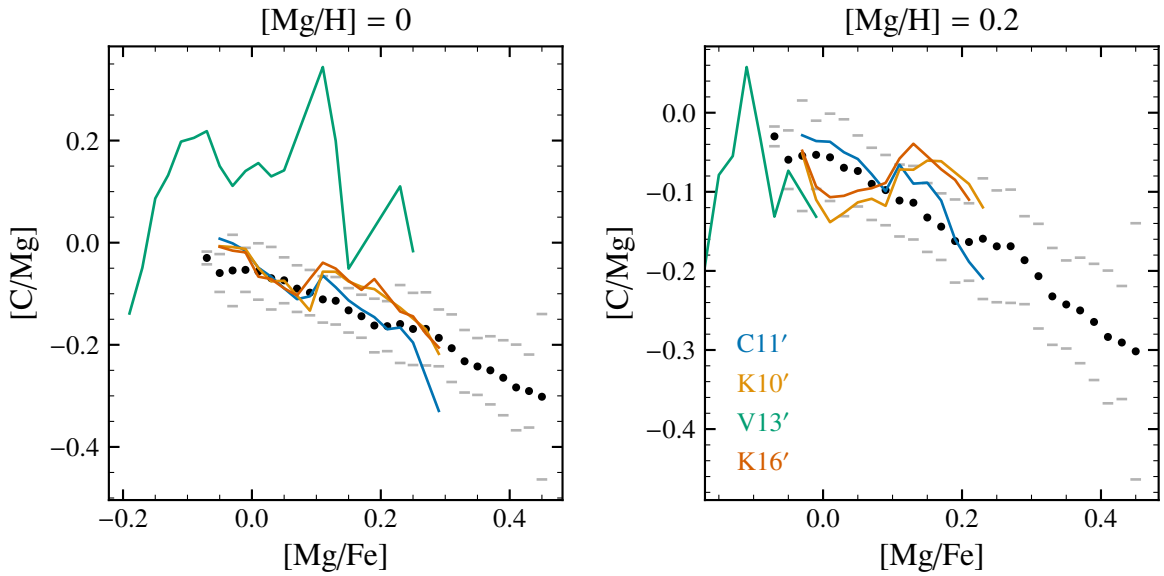


**Figure B1.** Same as 6 but comparing our fiducial model to our recommended z-dependent $y_C^{CC}$ model. A plot of the stars of our favored CCSNe model colored by radius. The contours represent the density of V+21 data. The model is given Gaussian scatter equivalent to the mean error in the abundances reported by APOGEE.